COMPDYN 2015
5th ECCOMAS Thematic Conference on
Computational Methods in Structural Dynamics and Earthquake Engineering
M. Papadrakakis, V. Papadopoulos, V. Plevris (eds.)
Crete Island, Greece, 25–27 May 2015

NUMERICAL SIMULATION OF THE LIMIT NON-LINEAR BEHAVIOUR OF UNREINFORCED STONE MASONRY UNDER IN-PLANE STATE OF STRESS FROM GRAVITATIONAL AND SEISMIC ACTIONS

G.C. Manos[1], L. Kotoulas[2] , V. Soulis[3], O. Felekidou[2]

[1] Professor and Director of the Lab. of Strength of Materials and Structures, Aristotle University
e-mail: {gcmanos@civil.auth.gr}

[2] Postgraduate student, Lab. of Strength of Materials and Structures, Aristotle University
e-mail: Κωτούλας Λάμπρος {kotoulaslambros@gmail.com}, {felekidou23@yahoo.gr}

[3] Dr. Civil Engineer, Lab. of Strength of Materials and Structures, Aristotle University
e-mail: {soulis@yahoo.com.gr}

Keywords: Stone masonry, In-plane behavior, Gravitational forces, Seismic actions, Limit non-linear behaviour, In-plane behaviour

Abstract. *Unreinforced masonry made of stone and low strength mortar has been used for centuries in forming the structural system of old type buildings as well as monumental structures (such as churches etc.) The behaviour of this type of structural systems that survive today, when subjected to the combined gravitational loads and seismic actions, is still of interest. In this framework, the present work tries to evaluate the limit-state in-plane behavior of stone masonry vertical structural elements. Initially, the basic aspects of a methodology are presented whereby the performance of vertical structural elements under seismic actions can be examined through a decomposition process whereby the demands at critical locations of individual piers, that the whole structural system is decomposed to, are compared with the corresponding bearing capacities in either in-plane shear/flexure or in out-of-plane flexure. Next, this methodology is applied to predicting with a reasonably good agreement the performance of stone masonry piers of two churches damaged by the recent Kefalonia-Greece 2014 earthquake. The possibilities offered by non-linear inelastic numerical analyses as alternative means for examining the performance of unreinforced stone masonry vertical structural elements is briefly presented. In addition, numerical simulation results are also presented making use of such non-linear inelastic numerical analyses. The predictions obtained through such non-linear inelastic numerical analyses toward predicting the measured behaviour of stone masonry specimens that were subjected in the laboratory to simultaneous compression and shear or diagonal compression had a reasonable level of success.*

1 INTRODUCTION

During the last thirty years various parts of Greece have been subjected to a number of damaging earthquakes ranging from Ms=5.2 to Ms=7.2 on the Richter scale. Some of these events, not necessarily the most intense, occurred near urban areas (Manos [7] and [10]). One of the most demanding tasks for counteracting the consequences of all these seismic events was the effort to ensure the structural integrity of old churches, that were built in periods ranging from 400 A.D. till today; in many cases they sustained considerable damage. Selected results and summary observations of the seismic behavior of a specific type of structural system are presented by Manos et al. [5, 6, 8]. This system is utilized in many churches belonging to the so called Basilicas. This structural system is one of the oldest structural forms and it is frequently utilized for Greek Christian Churches with a number of variations in plan and height. The "Basilica" structural system is of rectangular shape, formed by the peripheral walls; a semi-cylindrical apse is usually part of the East wall, whereas the interior is divided in a number of naves by longitudinal colonnades of various dimensions and shapes, as shown in figure 1a. The roofing system is mainly in the longitudinal direction; this roofing system at the central nave usually rises at a higher level than that of the side-naves; in this sense, it can be seen as an elevated extension of the interior colonnades. On the contrary, the roofing system that covers the side naves is partially supported on the peripheral walls and is usually lower than the roof of the central nave (figure 1b). In some instances this structural type takes the simplest form of one nave with no internal separations. This is also the form of rectangular old age masonry buildings with strong peripheral walls and weak internal separations.

Patras-Greece Earthquake 2008

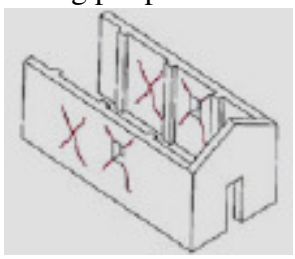

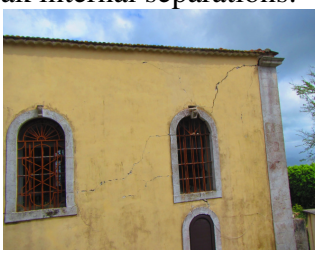

Kefalonia-Greece Earthquake 2014

Figure 1. Typical damage patterns of longitudinal walls

2 TYPICAL DAMAGE PATTERNS

When such structural formations are subjected to horizontal earthquake forces the longitudinal and transverse walls represent the main structural elements that resist these forces ([3]). Despite the fact that the total structural dynamic response is quite complex it is convenient to simplify this response for each one of these main resisting structural elements by decoupling it to in-plane and out-of-plane response that leads to a corresponding state of stress which acts together with the state of stress due to the gravitational forces. When the state of stress due the earthquake forces keeps increasing certain in-plane and out of plane limit strength values are reached that lead to corresponding modes of failure (figures 1, 2 and 3).

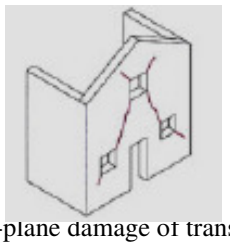

Typical in-plane damage of transverse walls

Kefalonia-Greece Earthquake 2014

Figure 2. Typical in-plane damage patterns for transverse walls

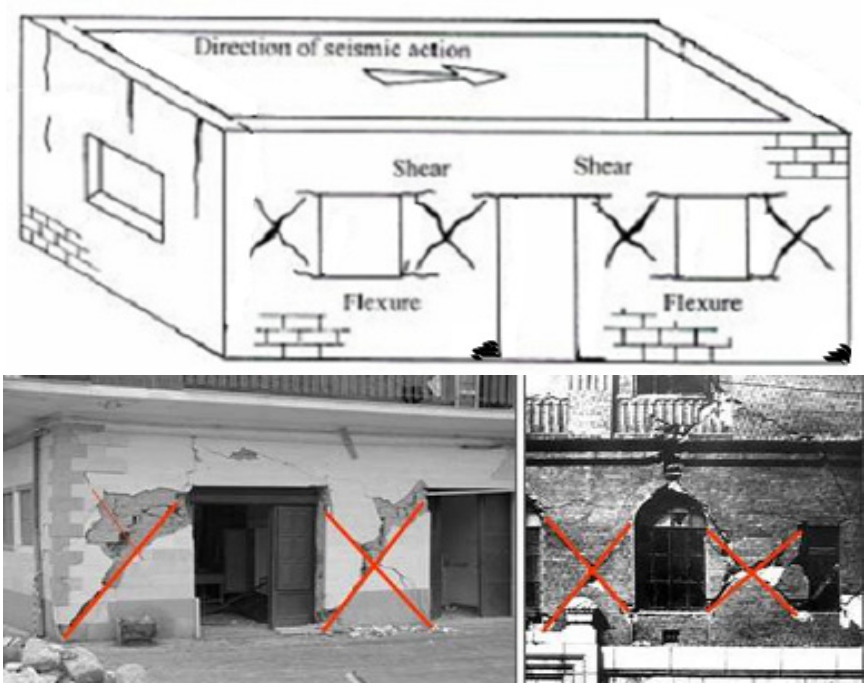

Figure 3. Typical in-plane damage patterns

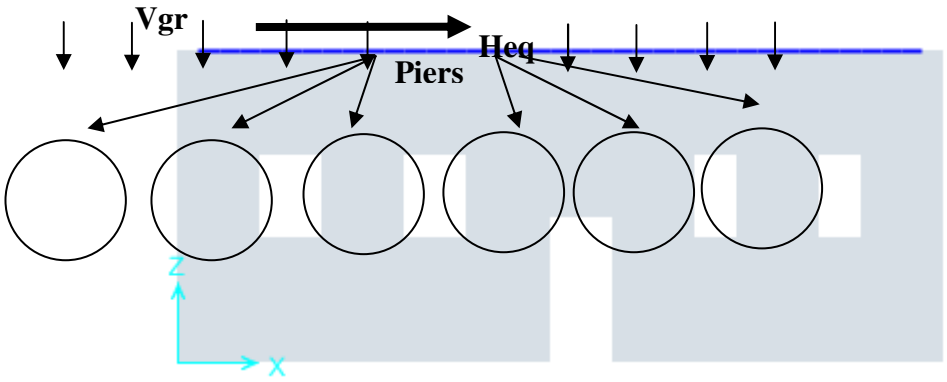

Figure 4. Decomposition of a masonry wall to piers between openings

3 THE STATE OF STRESS OF PIERS BETWEEN OPENINGS IN MASONRY WALLS

Figures 1, 2 and 3 depict such typical in-plane damage patterns for longitudinal and transverse masonry walls. Each one of the in-plane damage patterns that develops in either the longitudinal or the transverse walls arises from the fact that at a certain location the state of stress resulting from combination of the gravitational loads (Vgr) and the earthquake forces (Heq), as shown in figure 4, leads to a demand that exceeds the capacity at this location.

3.1 The decomposition of a masonry wall in a number of masonry piers

One way to deal with this problem is to be able to continuously reaching realistic estimates of the demands at each location and compare these demands with the corresponding capacities and in this way at every forcing level Heq have a continuous adjustment of the contribution of

each part of the wall in the total stiffness and strength and note all the important changes as well as the location where a certain strength limit is reached. This requires a non-linear analysis. For earthquake loads this non-linear analysis is usually performed by applying the horizontal earthquake forces in a step-by-step push-over way. This has been applied with reasonable success by Manos and Soulis for the church of Metamorphosi toy Sotiros in Zaborda, Kozani, Greece.

Alternatively, one can see each vertical wall as being composed by a number of masonry piers that are formed by door or window openings that are usually present, as indicated in figure . These piers usually form the weakest part of the structure. As was shown previously by figures 1 to 3, these piers are the locations where the most severe structural damage usually concentrates.

The demands that arise at each location can be found by various simple or complex methods of numerical approximations and is not part of the current study. In any case these demands can be seen as arising at the top of each individual pier that a vertical wall can be envisaged as being formed of. Thus, in this way each longitudinal and transverse wall is on its own by being composed of various vertical parts (piers) that together with the openings form each wall as a whole (figures 1 and 3). Following this decomposition of a wall to a sum of piers between openings it is on the conservative side to ignore the connections between the longitudinal and the transverse walls at the corner. Consequently each individual pier can be seen as a simple rectangular vertical structural element that is forced by the relevant stress resultants at its upper horizontal boundary and is supported in its lower horizontal boundary in a way capable to transfer axial forces as well as in-plane shear forces and bending moments at depending on the shear and flexural capacity of this lower boundary of the masonry wall, located at a distance equal to ***h*** form the upper boundary.

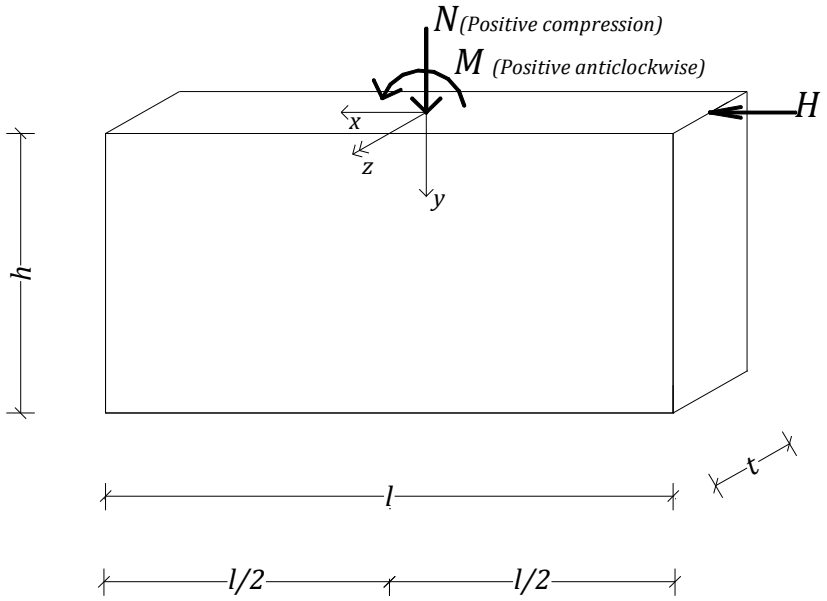

Figure 5. Single masonry pier being stresses in its upper boundary

Consequently, each one of the piers is considered as being stressed in-plane mainly in their upper horizontal boundary and is being supported at their lower horizontal boundary as shown in figure 5. Figure 5 depicts the geometry of such a masonry pier together with the in-plane loads (***N, H, M***) acting on its upper boundary. The stress resultants N_y, Q_y, M_y at an horizontal cross section located at a distance ***y*** from the top horizontal boundary of the pier are given below:

$$M_y = M + H\,y \quad , \quad N_y = M + lt\rho\, y \quad , \qquad Q_y = H \tag{1}$$

Where ρ is the specific gravity of the wall, l and t are the geometrical dimension of the pier as shown in figure 5. The calculation of the normal stress at this horizontal cross section is carried out as follows:

Having obtained the demands in every horizontal cross section of the pier in this way the performance of this pier can be evaluated next by comparing these demands with the corresponding shear and flexural capacities. Towards this objective it is essential to be able to approximate the state stress in any horizontal cross-section in terms distribution of axial stresses normal to this cross section and shear stresses parallel to the same cross-section. One particular complication for obtaining such realistic axial and shear stress distributions springs from the fact that masonry and especially old type stone masonry is constructed with mortar that is relatively much weaker in tension and shear than in compression. Moreover, the mortar is also much weaker in tension and shear than the masonry units that can be either man-made or formed from natural stone.

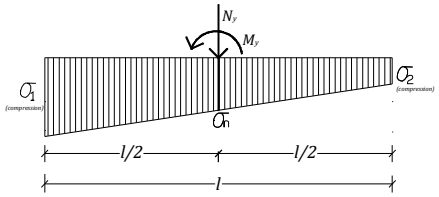

a. *Case 1*:

The normal stress distribution is compressive along all the length of the pier:

$$\sigma_1 \geq 0 \quad and\, \sigma_2 \geq 0$$

The largest normal stress value must be smaller than the masonry compressive strength f_{kd}

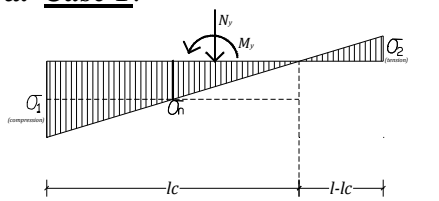

b. *Case 2*:

There is tension at the right zone of the cross section with stress σ_2 lower than the tensile limit stress f_{xk1d} ; consequently, the tensile zone is assumed being active:

$$\sigma_1 \geq 0\,; \sigma_2 < 0;\ |\sigma_2| \leq f_{xk1d}\ and\ \sigma_1 < f_{kd}$$

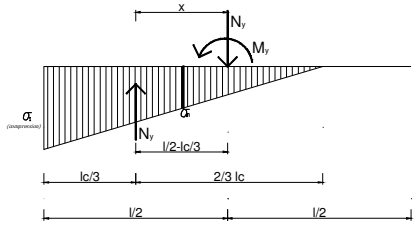

c. *Case 3*:

There is tension at the right fiber of the cross section, larger than the tensile limit stress f_{xk1d} ; consequently, the tensile zone is assumed being inactive:

$$\sigma_1 \geq 0\,; \sigma_2 < 0;\ |\sigma_2| \geq f_{xk1d}\ and\ \sigma_1 < f_{kd}$$

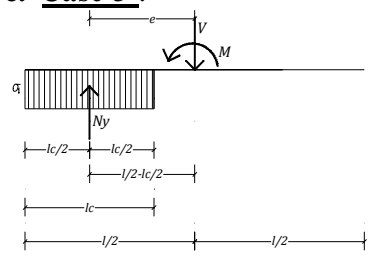

d. *Case 4*:

The tensile zone remains inactive but the compressive zone becomes narrower than before (towards developing flexural mode of failure):

$$\sigma_1 > 0\,; \sigma_2 < 0;\ |\sigma_2| \geq f_{xk1d}$$

and

$$e = \frac{M_y}{N_y l} \geq 0{,}45$$

Figure 6. Normal to the bed-joint axial stress distribution patterns

3.2 Predicting the shear bearing capacity of a pier against sliding

For this purpose use could be made of the provisions of Eurocode 6 [1]. For the masonry pier which is studied here the shear strength of the masonry (f_{vk}) is the minimum value of the following:

$$f_{vk} = f_{vk0} + 0.4\ \sigma_n \tag{2}$$

where σ_n is the value of the average normal stress, f_{vk0} the shear strength of the masonry for zero normal stress that is specified by the provisions of Eurocode 6 [1].

$$f_{vk} < 0.065\, f_b \tag{3}$$

where f_b is the compressive strength of the masonry unit.

$$f_{vk} < f_{vklim} \tag{4}$$

where f_{vklim} is the upper shear strength of the masonry, as it is specified by the national appendix of each member state.

The distribution of axial stress (σ_n) normal to a bed joint with thickness equal to the pier thickness that develops at this horizontal section is assumed to be one of the following four simple cases depicted in figures 6a to 6d, which are incorporated in many design provisions. In order to obtain the shear capacity against sliding one should properly chooses which of these four cases of normal stress distribution develops based on the geometry, the stress resultants (N_y, Q_y, M_y) and the masonry compressive and tensile strength values, f_{kd} and f_{xk1d} respectively. These strength values as well as the checks being performed are based on the provisions of Eurocode 6 [1]; however, provisions from other codes can be easily incorporated. Together with the normal stress distribution, the length of the compressive zone (l_c) is also calculated as well as the value of the average normal stress (σ_n), which is assumed to act in this compressive zone as depicted in figures 6a to 6d. Use is made of both the compressive zone length and the average normal stress value for calculating next the masonry shear strength (see equations 2 to 4).

3.3 Predicting the shear bearing capacity of a masonry pier against diagonal tension

` This is done based on the following formula (Eq. 5) given by Turnsek and Cacovic [8, 9, 10]. It is assumed that the tensile strength of the masonry $\sigma_t = f_{xk1}$ depends on the maximum average shear stress τ_{max} of a horizontal section of the masonry pier and on the average compressive stress $\sigma_d = \frac{N}{A}$ that develops on the same location where A the area of this section and N the compressive load.

$$\sigma_t = f_{xk1} = \sqrt{(\sigma_d/2)^2 + (b\,\tau_{max})^2} - \sigma_d/2 \tag{5}$$

Where b represents the shear stress distribution factor, which is related to the stress distribution on the section and the slenderness ratio of the wall. It can be assumed that $b = \frac{h}{l}$, where h is the height and l is the length of the pier. In this case $b = 1.5$ is the upper limit value and b

= 1 is the lower limit value. From the above relationship the value of τ_{max} can be obtained based on the values of $\sigma_t = f_{xk1}$ and σ_d:

$$\tau_{max} = \frac{f_{xk1}}{b}\sqrt{f_{xk1} + \sigma_d} \tag{6}$$

4 EVALUATING THE PERFORMANCE OF MASONRY WALLS WITH OPENINGS

Based on the above described procedures from predicting the bearing capacity of a masonry pier either against sliding or against diagonal tension the following steps can be followed in order to predict the expected performance of a given unreinforced masonry pier in terms of shear bearing capacity and expected mode of failure. The basis of such a prediction is to include in the expert system the most common modes of failure that such a structural element can develop under the in-plane loads shown in figures 7. Because the focus of this study are the modes of failure that are due mainly to the seismic actions the first checks try to identify the development of the following modes of failure:

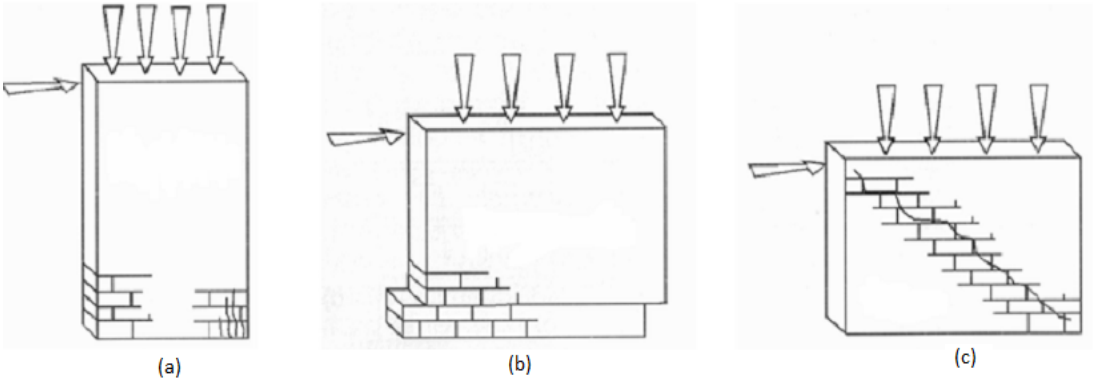

a) Flexural b) shear/sliding c) shear / diagonal tension

Figure 7. Typical in-plane failure modes, considered by the expert system, for individual piers subjected to gravitational forces and in-plane seismic actions.

a) The flexural mode of failure (figure 7a). This is done by assessing the distribution of the normal stress at a horizontal cross section, as explained before (figures 6a to 6d). At the same time the maximum compressive stress is also checked which must attain values below the limit compressive strength of the masonry (f_{kd}). If not, flexural failure is predicted.

b) The sliding mode of failure of a horizontal cross-section located either at the bottom or at mid-height of the pier (figure 7b). In doing so the simple Mohr-Coulomb friction is assumed as it is expressed by the provisions of Eurocode 6 (Eq. 2, [7]), for unreinforced masonry, as presented before. The shear/sliding capacity in this case is found based on the masonry sliding shear strength, presented before, and on the compressive zone length (l_c) (see figures 6a to 6d).

c) The shear/diagonal mode of failure (figure 7c); this is calculated from the combined state of stress for the pier, as outlined before. The objective here is to predict this shear/diagonal tension capacity based on the procedure that calculates the maximum shear/diagonal tension stress (Eq. 6).

Both procedures, which were described in 3.2 and 3.3, are incorporated in an expert system that can predict through steps a), b) and c) the bearing capacity of a given pier and the expected mode of failure [ ]. This is applied in the following cases that were selected from vertical masonry walls of two churches damaged during the recent 2014 Kefalonia-Greece earthquake sequence [ ].

These Basilica churches are Panagia at Chavriata and Agia Marina at Soullaroi. Both churches sustained heavy structural damage depicted in figures 8a and 8b, respectively. The dimensions in meters are also indicated in these figures. The examined by the expert system piers are the ones at the West transverse wall (façade) between the door at and the North and South walls (see figures 8a and 8b). The base shear forces for the two churches were obtained through a dynamic spectral analysis with an acceleration spectrum the one derived from the ground acceleration recorded by an accelerograph located at the floor of an old school at Chavriata. The distance between the Agia Marina at Soullaroi and Chavriata is less than two kilometers. Consequently, the same input response spectrum (q=1.5) was used for both churches (4 and 5 first eigen-modes for Ag. Marina and Panagia, respectively). Two types of soil were examined by introducing two-node links at the soil-foundation interface; hard soil conditions were assumed with link axial stiffness equal to 109KN/mm and soft soil conditions when this link axial stiffness value was equal to 24.5KN/mm

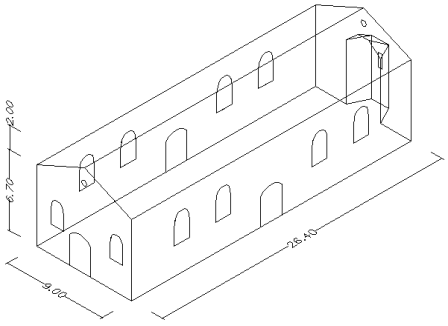

Figure 8a. Church of Panagia at Chavriata

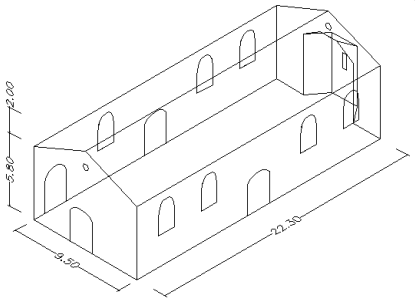

Figure 8b. Church of Agia Marina at Soullaroi

The shear demands when the seismic forces act in the transverse (y-y) North-South direction and thus subject the relatively short East or West masonry walls of these churches to in-plane seismic actions are listed in table 1. The listed values are the base shear demands in this direction for the whole church as well as the shear demand (Q) for the examined here masonry piers.

Table 1	***Shear demands based on the Chavriata response spectra in the East-West (y-y) transverse direction***	
Name of church	Base Shear (KN) for the whole Church, Hard Soil	Shear Q (KN) for the studied pier (l, t), Soft Soil
Agia Marina, Soullaroi	8828	1351 (4156mm x 750mm)
Panagia, Chavriata	16308	2330 (3600mm x 750mm)

Table 2	Compressive strength f_k (MPa)	Shear Strength f_{vko} (MPa)	Axial tensile strength normal/parallel to bed-joint f_{xk1}/f_{xk2} (MPa)
Limit values	3,50	0,16	0,15/0,6

Table 2 lists the assumed mechanical characteristics for the stone masonry in terms of compressive, shear and tensile strength values. f_{vko} is the shear strength of the stone masonry when the normal stress is zero; fvko was assumed to be equal to 0.160 N/mm2. The values listed in table 4 were assumed to be valid for both churches based on relevant strength values employed in similar studies [1, 3, 4, 5, 11, 12, 15, 16, 17]. However, the necessity to quantify such limit value through tests based on in-situ samples must once more be underlined (see section 5).

Table 3	***Shear demands based on the Chavriata response spectra in the East-West (y-y) transverse direction***	
Name of church	**Demands** on the Pier N_y (KN) / M_y (KNm) / and Q_y (KN)	**Shear Capacity** Q_{sl} (KN) / against sliding Q_{dg} (KN) against diagonal failure
Agia Marina, Soul-laroi	560 / 325 / **1351**	864 / **694** (KN)
Panagia, Chavriata	1059 / 475 / **2330**	725 / **779** (KN)

Next, the expert system [18] will be utilised in order to evaluate the performance of the piers of the West walls for both churches that are formed from the door openning. Table 3 lists the more severe demands for these piers in terms of stress resultants N_y, M_y, and Q_y, as these demands resulted from the numerical analyses with horizontal seismic forces equal to the base shear values listed in table 1. Together with these demands the shear capacity values of the examined piers are also listed in this table, against sliding and against diagonal failure, as they were found by applying the developed expert system. As can be seen for the piers of both churches the diagonal failure is predicted. Moreover, it can also be seen that the values of the shear capacity / demand ratio based on the values of table 3 are equal to 0.51<1 for the church of Agia Marina at Soullaroi, and 0.33<1 for the church of Panagia at Chavriata. Again, through this process of evaluating the performance of the examined piers the shear damage predictions are in agreement with the observed performance.

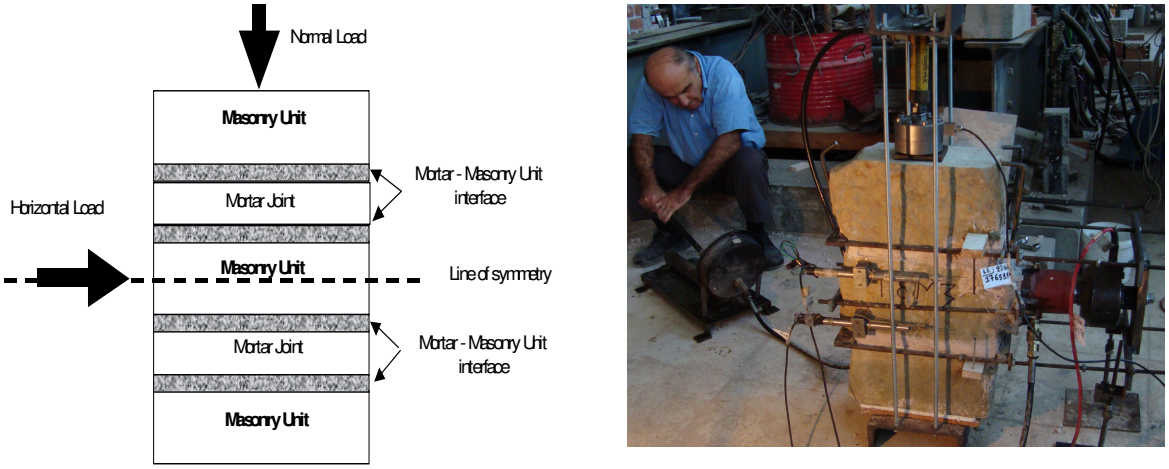

Figure 9. Test arrangement for a triplet test

5 SIMPLE TESTS FOR OBTAINING THE SHEAR STENGTH OF STONE MASONRY PIERS

5.1 The triplet test

This a relatively simple and well known tests whereby two mortar joints are subjected to axial normal stress (σ_n) that remains at a constant amplitude throughout all the duration of the test. The horizontal load is applied in a way as to produce the desired sliding failure between the stones and the mortar joints as it is indicated in figure 9. The objective of such tests is to be able to quantify the parameters included in the Mohr-Coulomb criterion as expressed by equation 2.

Mohr Coulomb failure criterion fv = fvo + 0.45 σ
fvo = 0.12 Mpa

	Normal Stress σ (Mpa)	Predicted fv = fvo + 0.45 σ (Mpa)	Measured value fv (Mpa)	Ratio Measured fv / Predicted fv
Sample 1	0.53	0.359	0.396	1.103
Sample 2	0.61	0.395	0.41	1.038
Sample 3	0.46	0.327	0.305	0.933
Sample 4α	0.30	0.255	0.20	0.784
Sample 4β	0.54	0.363	0.375	1.033

Figure 10a. Verification of the Mohr-Coulomb criterion

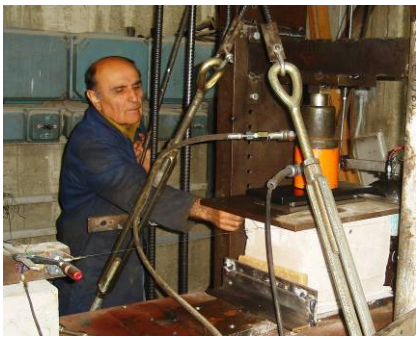

Figure 10b. Experimental set-up

Figure 9c. Sliding mode of failure

Figure 9d. Sliding mode of failure

A more complex extension of the above triplet test is the one shown in figures 10 to 10d where a short stone masonry pier with dimensions in plan somewhat larger than its height ia again subjected simultaneously to constant axial normal stress *(σ_n)* whereas at the same time a continuously increasing horizontal load tries to produce a shear mode of failure for this short pier. A number of short stone masonry specimens were built at the laboratory of Strength of Materials and Structures of Aristotle University using lime mortar and natural stones. The lime mortar had such a composition as to be representative of old relatively weak mortars commonly used in the past. A series of such samples were tested accompanied by constant compression with variable shear as shown in figure 10b. This set-up was designed in an effort to record the shear force at a limit state which represented the failure of the mortar bed-joint as depicted in figures 10c,d. Based on these experimental results, the Mohr-Coulomb limit state criterion (figure 10a, equation 2) can be approximately quantified.

Following these initial samples, another sequence of tests will be performed aimed at quantifying the Mohr-Coulomb failure envelope representing old stone masonry that was injected in the framework of a mild retrofitting scheme. The injected mortar should be of such a

composition as: a) to be compatible with the existing materials b) to be able to fill the existing voids and c) to result in higher strength values.

5.2 Diagonal tension of masonry piers.

This type of tests is shown in figure 11 for a brick masonry pier. In the usual test set-up such masonry piers having equal length and height are placed in a diagonal orientation and the compressed in order to produce in this way the diagonal tension mode of failure, which was described in section 3.2. This testing arrangement is relatively difficult to be applied at stone masonry piers (figure 12). For such piers testing arrangement described in the next section is usually adopted.

Figure 11. Brick masonry pier being subjected to diagonal compression/tension at the laboratory.

Figure 12. Stone masonry pier being subjected to diagonal compression/tension in-situ.

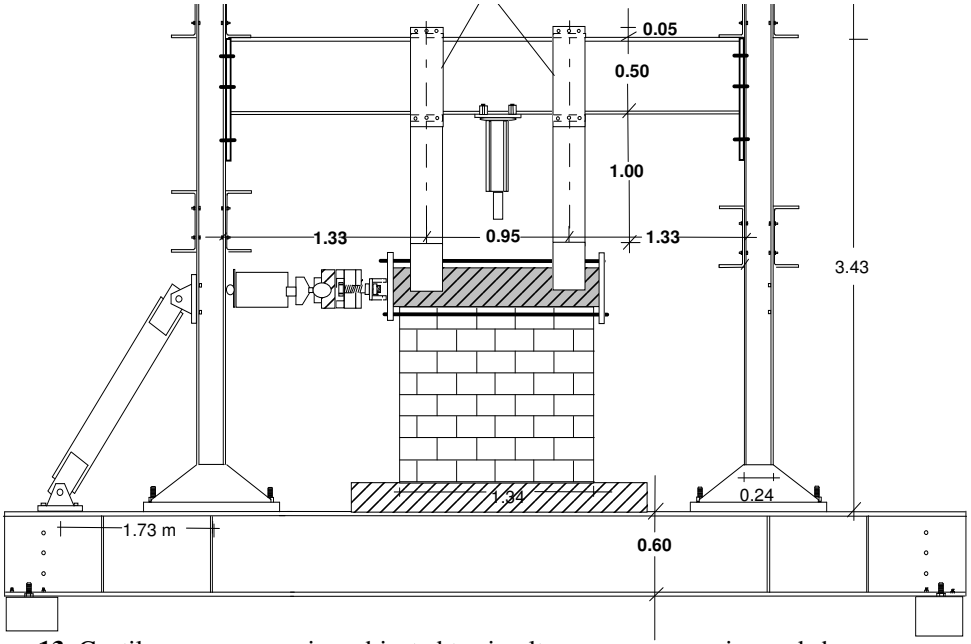

Figure 13. Cantilever masonry pier subjected to simultaneous compression and shear

5.3 Cantilever masonry piers being subjected to simultaneous compression and shear.

This type of tests is shown in figure 13. This loading arrangement reproduces under controlled laboratory conditions the state of stress described by equation 1 and shown by figure 6.

The vertical load is applied at a desired level and kept constant throughout the test whereby the horizontal load is progressively increased. More advanced tests of this type include the variation of the horizontal load in a cyclic way thus simulating a seismic type of loading. The objective of this type of test is to be able through all the measured response parameters to identify the state of stress distribution for this pier and to be able to account for its mode of failure validating in this way one of the failure criteria presented in sections 3.2. and 3.3.

6 NUMERICAL SIMULATIONS

There is a variety of numerical simulations that can be performed in order to predict in a realistic way the performance of structures built with stone masonry. Elastic dynamic spectral numerical analyses try to obtain the demands in the various masonry components for a simple or complex structural system and then evaluate their performance by applying well established failure criteria or code provisions as was presented in section 3. Alternatively, non-linear inelastic "push-over" type of numerical analyses were also performed whereby a masonry structure is subjected first to the permanent vertical loads and then the seismic horizontal forces are applied through a realistic form of horizontal displacement pattern in order to obtain the bearing capacity of the structure under such a horizontal seismic-type loading [12].

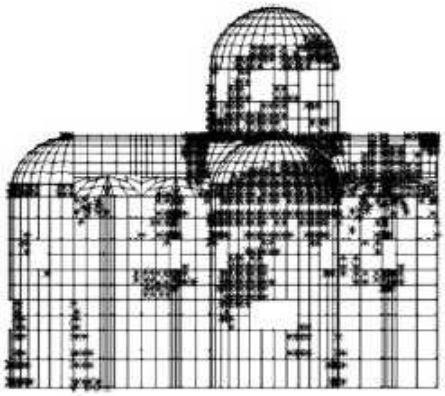

Figure 14. Predicted limit state locations

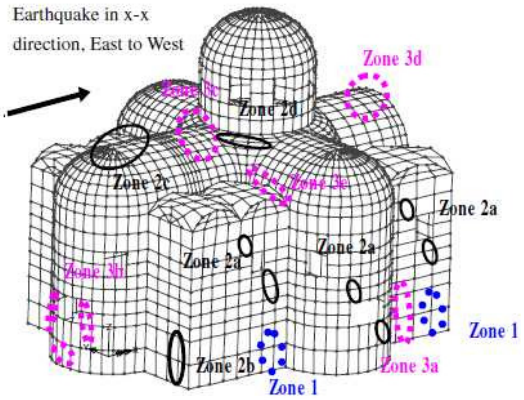

Figure 15. Predicted modes of failure

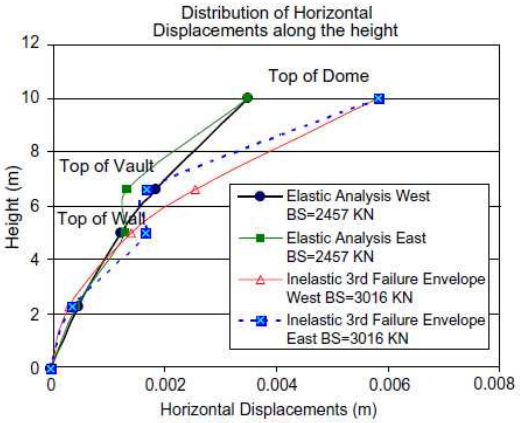

Figure 16. Displacement patterns along the height

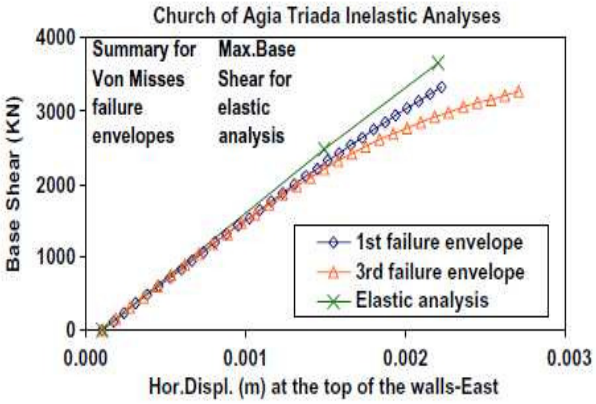

Figure 17. Top displacement versus base shear response

Summary results are shown in figures 14 to 17 from such an inelastic "push-over" type of numerical analysis. In figures 14, the location where the limit state conditions are predicted is shown whereas in figure 15 the predicted modes of failure for the peripheral walls of a Post-

Byzantine church are depicted as they resulted from this push-over non-linear inelastic type of analysis. These predictions are based on realistic parameters of the incorporated in these non-linear numerical analyses of the Modified Von-Misses failure criteria for the various masonry components [12]. Zones of tensile failure (3a, 3b, 3c, 3d), zones of compression/tension failure (2a, 2b, 2c, 2d) and zones compression/compression failure (zones 1) are predicted from these analyses and are shown in figure 15. In figure 16 the distribution of the horizontal displacement along the height of this church as it results from an elastic and non-linear inelastic numerical analysis. Finally, the response of the examined structural system in terms of horizontal displacement at the top of the roof of this church against the base shear is depicted in figure 17 as it resulted either from the elastic or the inelastic numerical analyses.

6.1 Numerical simulation of the triplet test for short stone masonry piers.

In figures 18 to 21 the numerical simulation of the behaviour of the short pier and its loading conditions, described in sub-section 5.1, is depicted utilizing the ABAQUS commercial software package [13]. The numerical prediction of the bearing capacity of this pier in terms of shear stress is shown in figure 20 and it compares quite well with the measured maximum shear capacity that was observed during the cyclic test for this short pier (figure 21). Similarly, in figure 22 predicted by the non-linear inelastic analyses plastic strains are shown and can be compared with the observed damage pattern for the short pier that is shown in figure 23. As can be seen good agreement can be observed. Finally, figure 24 depicts the distribution of the principal tensile stresses that compares well both with the plastic strain distribution and the observed damage

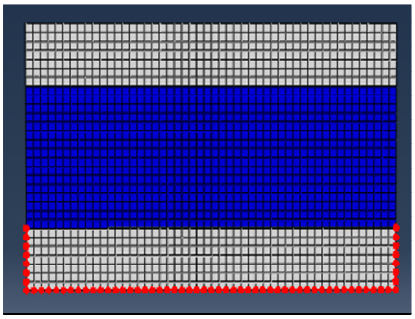

Figure 18. Fixing the low part of the short pier numerical simulation in the same way that the actual test specimen was supported.

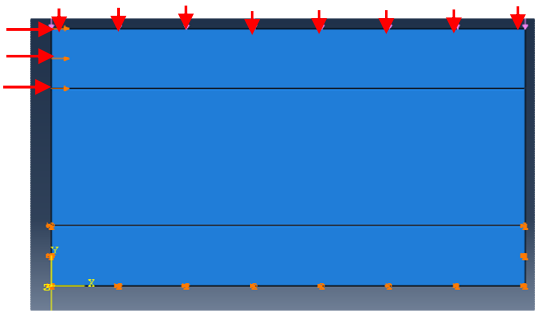

Figure 19. Fixing of the low part of the numerical simulation of the short pier in the same way that the actual test specimen was supported together with the application of uniform compression at the upper boundary equal to 0.16MPa.

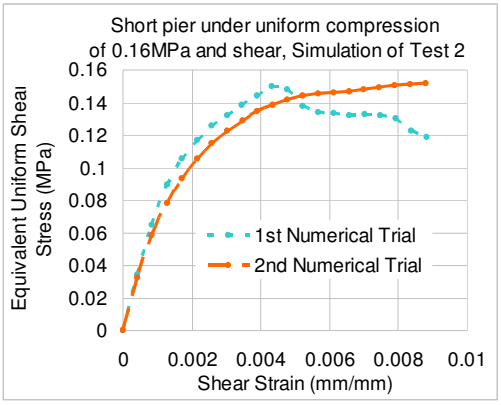

Figure 20. Numerical prediction of the monotonic response of the short pier in terms of shear stress (τ) /shear strain (γ) with simultaneous normal compressive stress 0.16MPa

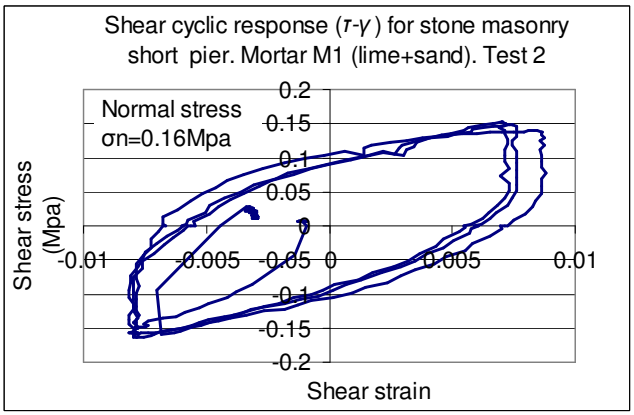

Figure 21. Measured cyclic response of the short pier in terms of shear stress and shear strain when it is simultaneously compressed with a normal stress equal to 0.16MPa

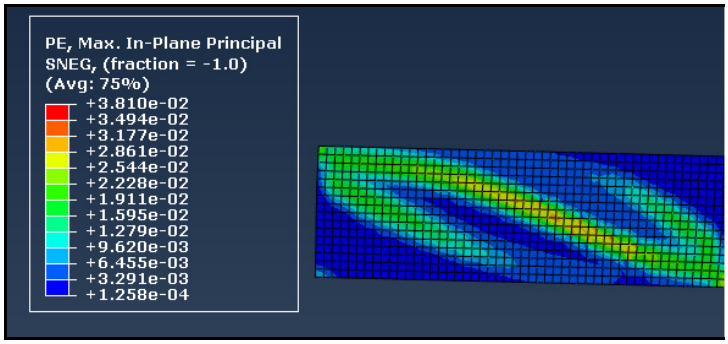

Figure 22. Distribution of predicted plastic strains

Figure 23. Observed damage patterns of the short pier

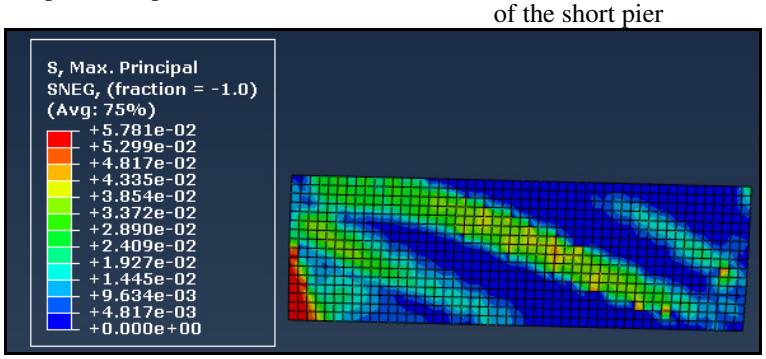

Figure 24. Distribution of tensile principal stresses at maximum load

6.2 Numerical simulation of a stone masonry pier subjected to diagonal compression

An unreinforced masonry wallette made of low quality three-leaf stone masonry with a length of 0.70 m a height of 0.90 m and a thickness 0.50 m was compressed diagonally as shown in figure 24. This is a numerical simulation of specimen 4 from an experimental sequence described in detail by Vintzileou [14] that tested 8 stone masonry specimens; three of those were in axial compression and 5 in diagonal compression. All the information provided in [14] was utilized in this numerical simulation. The ABAQUS [13] commercial software package was employed for these numerical analyses.

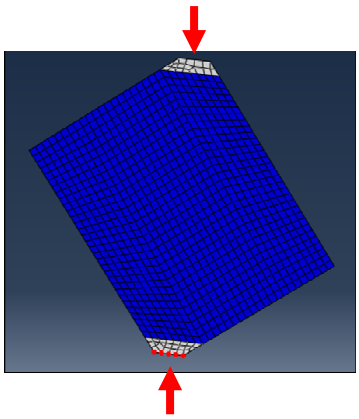

Figure 24. Diagonal compression

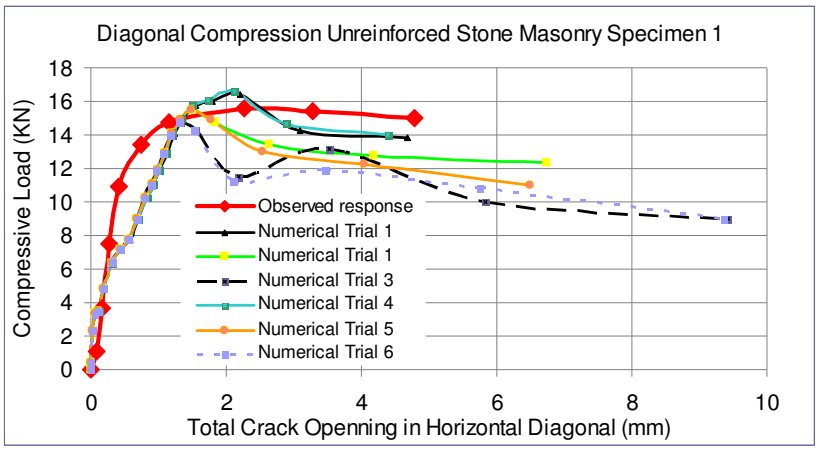

Figure 25. Comparison of numerical predictions with test results for the diagonal compression test

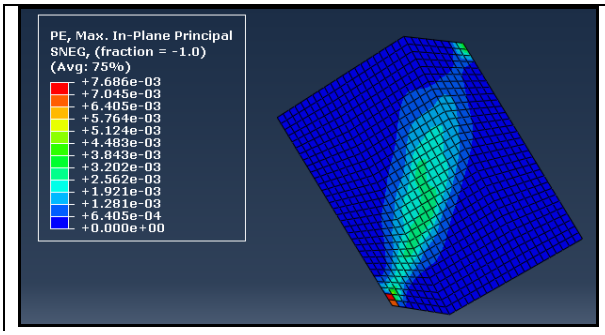

Figure 26. Distribution of predicted plastic strains

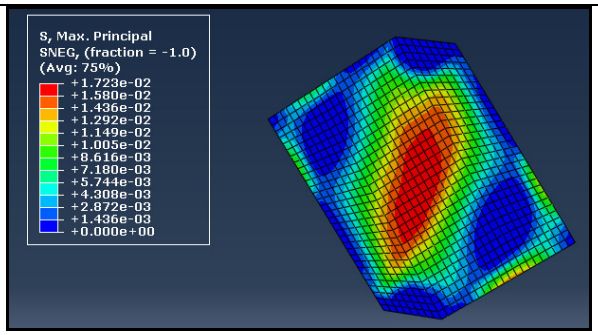

Figure 27. Distribution of tensile principal stresses at maximum load

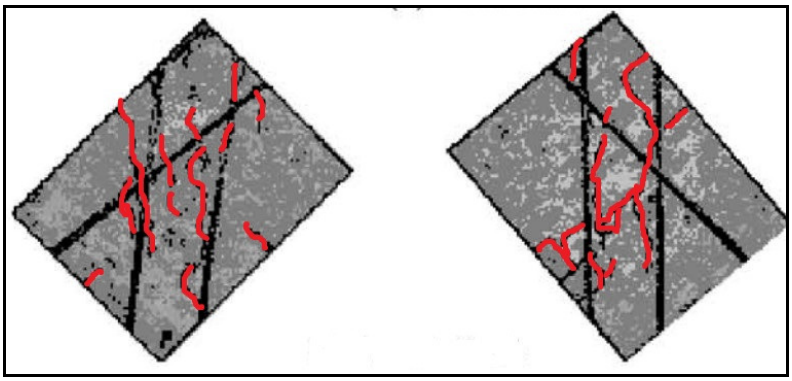

Figure 28. Observed cracking patterns of the diagonal compression specimen [14]

6.3 Numerical simulation of a cantilever pier with simultaneous compression and horizontal load.

A stone masonry pier is examined here with a length equal to ***l***=1500 mm height ***h***=1400 mm and thickness ***t***= 500 mm. This pier is subjected to its upper boundary with a uniform compressive pressure equal to 0.1MPa. The special gravity of this masonry wall is considered equal to 2.20 tn/m3. Because this pier is assumed to be constructed by a relatively weak masonry therefore the Young's modulus for the horizontal load is presumed to be equal to 200 MPa. The horizontal load results from the imposed horizontal displacement at the upper boundary that reaches at the final stages of this numerical study to have a value equal to 30mm. The material properties listed in table 2 were considered together with the Mohr-Coulomb criterion given in equation (1), e.g. $f_{vk} = f_{vk0} + 0.4\ \sigma_n$

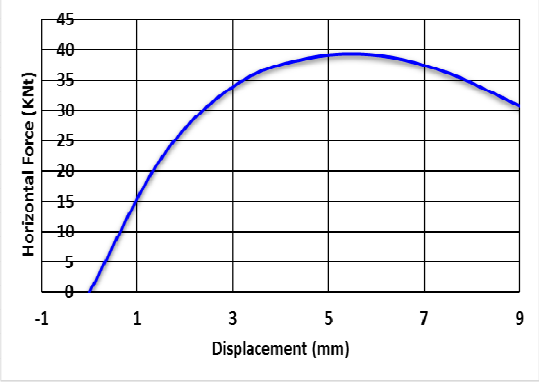

Figure 29. Horizontal load versus horizontal displacement of the studied cantilever pier.

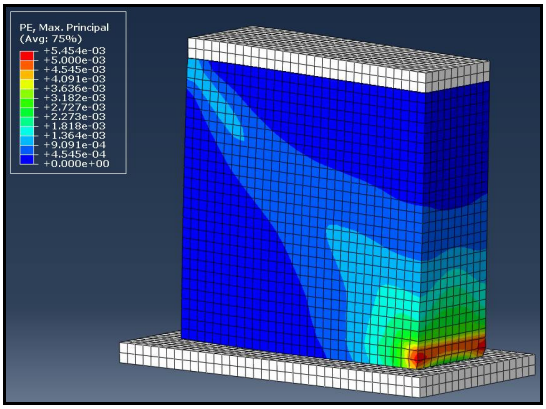

Figure 30. Plastic strains during the response of the pier beyond the maximum load.

Figure 29 depicts the horizontal load versus horizontal displacement response at the top of studied pier whereas figure 30 depicts the plastic strains that develop at the right bottom toe of the pier when it reaches horizontal displacement levels at the top beyond the maximum load. Moreover, figures 31 the overall horizontal and vertical uplift displacement patterns of this pier at maximum load. Finally, figures 32 and 33 depict the distribution of the axial stresses normal to the bed joint and the principal tensile stresses, respectively,

.

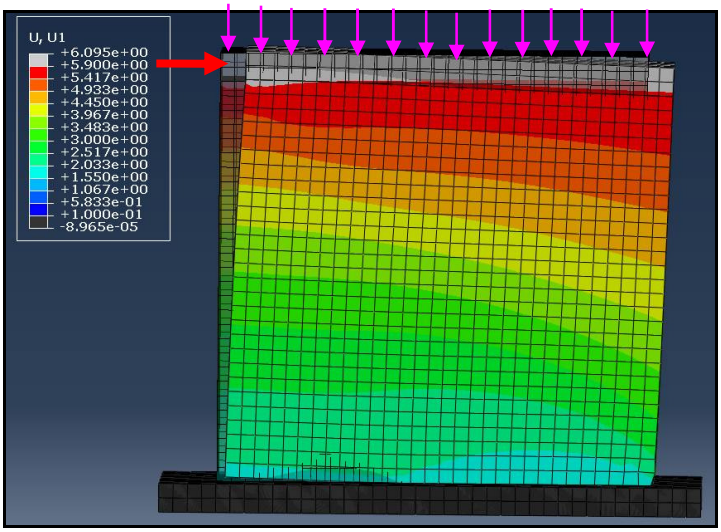

Figure 31. Horizontal sliding displacements at maximum load together with partial vertical uplift

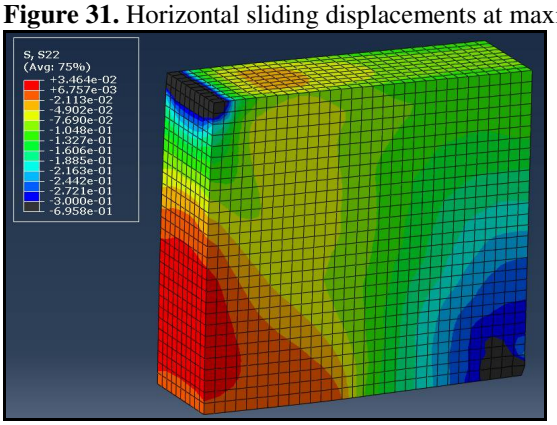

Figure 32. Distribution of axial stresses normal to the bed joints

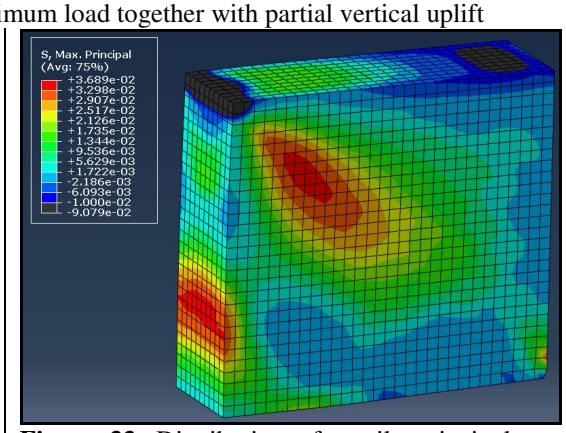

Figure 33. Distribution of tensile principal stresses at maximum load

As can be seen from these figure, the numerical simulation of the behaviour of this pier, under the simultaneous action of the constant vertical compression and the horizontal force at the top of the pier (figure 31), results in the complex state of stress described in sections 3.1. and 3.2. The resulting pattern of the horizontal and vertical uplift displacements are compatible with the assumed limit-state tensile and shear strength values. The shear capacity of this pear is governed by the sliding response rather than the diagonal tensile bearing capacity, despite the fact that figure 33 shows the initiation of such a diagonal tensile crack pattern.

7 CONCLUSIONS

- The performance of masonry structures under seismic actions can be examined through a decomposition process whereby the demands of critical locations of individual piers that the whole structural system is decomposed to are compared with the corresponding bear-

ing capacities in either in-plane shear/flexure or in out-of-plane flexure. The relevant methodology is outlined that forms the basis of an expert system which was developed for this purpose.

- When this methodology is applied for predicting the performance of stone masonry piers of two churches damaged by the recent Kefalonia-Greece 2014 earthquake, good agreement could be found between shear damage predictions and the observed performance.
- The importance of employing realistic limit-state criteria to be utilized in assessing the bearing capacities of unreinforced stone masonry structural elements is then out-lined together with a summary presentation of relatively simple laboratory testing that can be employed for this purpose.
- The possibilities offered by non-linear inelastic numerical analyses as alternative means for examining the performance of unreinforced stone masonry structural elements is briefly presented. In addition, numerical simulation results are also presented making use of such non-linear inelastic numerical analyses. The objective here is to numerically simulate the performance of masonry specimens that were subjected to relatively simple laboratory testing. Successful predictions of the observed performance are means to increase the confidence in these numerical tools before employing them in more complex structural formations.
- The predictions obtained through such non-linear inelastic numerical analyses toward predicting the measured behaviour of stone masonry specimens that were subjected to simultaneous compression and shear or diagonal compression can be considered that had a reasonable level of success.

ACKNOWLEDGEMENTS

The authors would like to thank Civil Engineer N. Parcharidis for his assistance during the numerical simulations.

REFERENCES

[1] Manos G. C., (2011) “Consequences on the urban environment in Greece related to the recent intense earthquake activity”, Int. Journal of Civil Engineering and Architecture, Volume 5, No. 12 (Serial No. 49), pp. 1065–1090.

[2] Provisions of Greek Seismic Code with revisions of seismic zonation”, Government Gazette, Δ17α /115/9/ΦΝ275, No. 1154, Athens, 12 Aug. 2003.

[3] Manos G., Soulis V., Felekidou O., Matsou V. (2010) “A Numerical Investigation of the Dynamic and Earthquake Behaviour of Byzantine and Post-Byzantine Basilicas”, 9th U.S. and 10th Canadian Earthq. Eng. Conf., Canada.

[4] Manos, G.C, Kotoulas, L., Matsou, V., Felekidou, O. “Dynamic behaviour of Greek Post-Byzantine churches with foundation deformability and evaluation of their earthquake performance”, CompDyn2013, 12-14 June 2013, Greece.

[5] Manos G.C., Soulis V., Karamitsios N. (2012) "The Performance of Post-Byzantine churches during the Kozani-1995 Earthquake – Numerical Investigation of their Dynamic and Earthquake Behavior", 15WCEE, Portugal.

[6] Gulkan P., Clough R.W., Manos G.C. and Mayes R.L., (1990), "Seismic Testing of Single-story Masonry Houses : Parts 1&2", Journal of Str. Eng. ASCE, Vol. 116, No 1, January 1990, pp. 235-274.

[7] European Committee for Standardization, Euro-code 6 (2005); "Design of Masonry Structures, Part 1-1:General Rules for Building. Rules for Reinforced and Un-reinforced Masonry", EN 1996-1-1:2005.

[8] Turnsek V, Cacovic F (1971) Some experimental results on the strength of brick masonry walls. In: Proceedings of the 2nd international brick-masonry conference. British Ceramic Society, Stoke-on-Trent, pp 149–156

[9] Bernardini A, Modena C, Turnsek V, Vescovi U (1980) A comparison of three laboratory test methods used to determine the shear resistance of masonry walls" Proc. 7th WCEE, vol 7, IAEE, Istanbul, pp 181–184.

[10] Tomaževič M., 2009 "Shear resistance of masonry walls and Eurocode 6: shear versus tensile strength of masonry", Materials and Structures, August 2009, Volume 42, Issue 7, pp 889-907

[11] Manos G.C. & Kozikopoulos E. , (2015) "The dynamic and earthquake response of Basilica Churches in Kefalonia-Greece including soil-foundation deformability and wall detachment", CompDyn2015, Krete-Greece, 2015.

[12] Manos G.C., Soulis V., Diagouma A. (2008) "Numerical Investigation of the behaviour of the church of Agia Triada, Drakotrypa, Greece", Journal in Advances in Engineering Software 39, 284-300.

[13] Hibbitt, Karlsson, Sorensen. Inc. ABAQUS user's manual volumes I–V and ABAQUS CAE manual. Version 6.10.1. Pawtucket, USA; 2010.

[14] Vintzileou, E. "Effect of Timber Ties on the Behavior of Historic Masonry", American Society of Civil Engineers, Journal of Structural Engineering, Vol. 134, No. 6, June 1, 2008. ©ASCE, DOI: 10.1061/ (ASCE) 0733-9445 (2008) 134:6(961)

[15] G.C Manos, V. Soulis, N. Karamitsios, O. Felekidou, Numerical Simulation of the Dynamic and Earthquake Behaviour of Greek Post-Byzantine Churches with and without Base Isolation", PROHITECH 2009, 21 to 24 June 2009, Rome, Italy.

[16] G. C. Manos & N. Karamitsios , "Numerical simulation of the dynamic and earthquake behavior of Greek post-Byzantine churches with and without base isolation", Earthquake Engineering Retrofitting of Heritage Structures, Design and evaluation of strengthening techniques, pp. 171-186, Edited By: S. Syngellakis, Wessex Institute of Technology, UK, ISBN: 978-1-84564-754-4, eISBN: 978-1-84564-755-1, 2013.

[17] George C. Manos and Lampros Kotoulas "Earthquake Performance of Greek Post-Byzantine Churches with Foundation Deformability " Proc. 2nd Int. Conf. on Protection of Historical Constructions, pp. 297-303, 2014, ISBN 978-975-518-361-9.

[18] G. C. Manos, L. Kotoulas, O. Felekidou, S. Vaccaro and E. Kozikopoulos, "Earthquake damage to Christian Basilica Churches – Application of an expert system for the preliminary in-plane design of stone masonry piers", Int. Conf. STREMAH 2015.